Renormalization Group for Viscous Fingering with Chemical Dissolution

Takashi Nagatani,[1,2] Jysoo Lee,[1] and H. Eugene Stanley[1]
[1]*Center for Polymer Studies and Department of Physics, Boston University, Boston, Massachusetts 02215*
[2]*College of Engineering, Shizuoka University, Hamamatsu 432, Japan*
(Received 26 June 1990)

We study the evolution of patterns formed by injecting a *reactive* fluid with viscosity μ into a two-dimensional porous medium filled with a *nonreactive* fluid of unit viscosity. We treat the "mass-transfer limit," in which the time scale of the chemical reaction between the injected fluid and the porous media is much faster than the time scale of reactant transport. We formulate a three-parameter position-space renormalization group and find two crossovers: (1) from the first diffusion-limited-aggregation (DLA) to the Eden point—due to finite viscosity, and (2) from the Eden to the second DLA point—due to chemical dissolution. We also calculate the crossover exponent and the crossover radius.

PACS numbers: 68.70.+w, 05.40.+j, 47.70.Fw

The formation of dissolution patterns, by injecting a *reactive* fluid into a soluble porous medium filled with a *nonreactive* fluid, has been studied experimentally and computationally by Daccord and Lenormand.[1,2] They noted the connection between this process and the viscous fingering phenomenon, and also found that the patterns formed at high injection rate by the chemical dissolution process have the same form—and fractal dimension—as diffusion-limited aggregation (DLA).[3] The underlying mechanism for the formation of dissolution patterns involves the flow of liquid in the porous medium coupled with the chemical reaction between the injected fluid and the medium. Daccord[1] has proposed a simulation model that introduces a cumulative erosion process which broadens the branches of the cluster. The patterns obtained from the simulation are similar to the experimental ones.

Open questions include the asymptotic behavior of the dissolution patterns and their dependence upon such parameters as injection pressure and viscosity of the injected fluid. Chemical dissolution phenomena may be of particular interest in the domain of *biological physics,* where recently patterns have been discovered—such as the retinal vasculature and retinal neuron morphology —which resemble DLA both qualitatively *and* quantitatively.[4]

Here we address these open questions by developing a three-parameter position-space renormalization-group (PSRG) method. We find that the asymptotic behavior in this problem is characterized by two distinct crossovers: (1) one from DLA clusters to compact clusters (due to the finite viscosity ratio), and (2) another from compact clusters to DLA clusters (due to the chemical dissolution). Moreover, we find that the crossover phenomena depend on the injection rate.

Pattern formation by reactive injection fluid must be studied in two separate regimes.[5] The regime treated here is when the time scale of the chemical reaction is much smaller than those of the fluid motion (convection and diffusion). We call this regime the "mass-transfer-limited regime," since the speed of the chemical reaction is dominated by the supply of the reactive fluid. The other regime, where the time scale of the chemical reaction is much larger, is called "the reaction-limited regime."

The basic equations that describe the system are

$$\nabla\cdot[M_D\nabla P_D]=0 \tag{1a}$$

for the displaced fluid, and

$$\nabla\cdot[M_I(x,t)\nabla P_I]=0 \tag{1b}$$

for the injected fluid, where P_D and P_I indicate the pressures, and M_D and M_I the mobilities of the displaced and the injected fluids. The mobility of the injected fluid, $M_I(x,t)$, depends on position and time, and is governed by the cumulative erosion process. In the situation when the chemical reaction is much faster than the time scale of reactant transport, this erosion is controlled by the mass transfer.

We propose that the time evolution of the mobility is given by an equation similar to that used in Ref. 1,

$$M_I(x,t)=\mu^{-1}(1+\{q[t-t_0(x)]\}^{\beta}). \tag{2}$$

Here t is the total time, $t_0(x)$ the time when the injected fluid touches a site at position x, μ the viscosity of the injected fluid, and q the flow rate. In Ref. 1, it is argued that the parameter β is $\frac{3}{2}$ if the dissolution kinetics is limited by molecular diffusion. Equation (2) can be used to describe a cumulative erosion process that broadens the branches of the cluster. The pore size of the cluster increases with time after the injection fluid reaches point x. However, at the late stages of the dissolution process, the dissolving power is limited by the finite concentration of the reactant—the width of the branches cannot increase forever, due to the "spending" of the reactant. This effect can be studied by modifying the flow rate q in Eq. (2). In general, q is dependent not only on the flow rate, but also on the concentration of the reactant. The effect of a finite reactant concentration is not taken into account in the present model, but we expect that a finite concentration may serve to stabilize the pattern—favoring the Eden limit.

The boundary conditions on the interface are given by

$$P_D=P_I\,,\quad v_n=-M_D\hat{\mathbf{n}}\cdot\nabla P_D=-M_I\hat{\mathbf{n}}\cdot\nabla P_I\,, \tag{3}$$

where v_n is the normal velocity of the interface and $\hat{\mathbf{n}}$ the unit vector normal to the interface. Without losing generality, we set $M_D = 1$. It is convenient to describe the system using the language of the dielectric breakdown model. In this language, the conductance of the injected (displaced) fluid bond corresponds to the mobility of the injected (displaced) bond. Also, the electric field corresponds to the pressure field.

We consider the diamond hierarchical lattice (Fig. 1), and apply a constant current $q = q_0$ between the bottom and the top of the lattice. We distinguish three types of bonds: (1) injected fluid bonds (thick lines which form clusters), (2) *displaced fluid bonds* (thin lines), and (3) *growth bonds* (wavy lines on the perimeter of the cluster).

The conductances of the injected fluid, displaced fluid, and growth bonds are σ_I, 1, and σ_G, respectively. We now shall present the renormalization-group equations for the conductances of the surface and cluster bonds, for the total current, and for the time increment; the full derivation, which will be presented in a future publication, follows the method outlined in Ref. 6.

We partition the whole cluster into cells of size 2, and replace these cells with "renormalized" bonds. Thereby, generation n is renormalized to generation $n-1$. When the injected fluid bonds span the cell, we renormalize into *injected fluid bonds.* If a cell does not contain an injected fluid bond, we renormalize into a *displaced fluid bond.* When the injected fluid bonds do not span the cell, we renormalize into *growth bonds.*

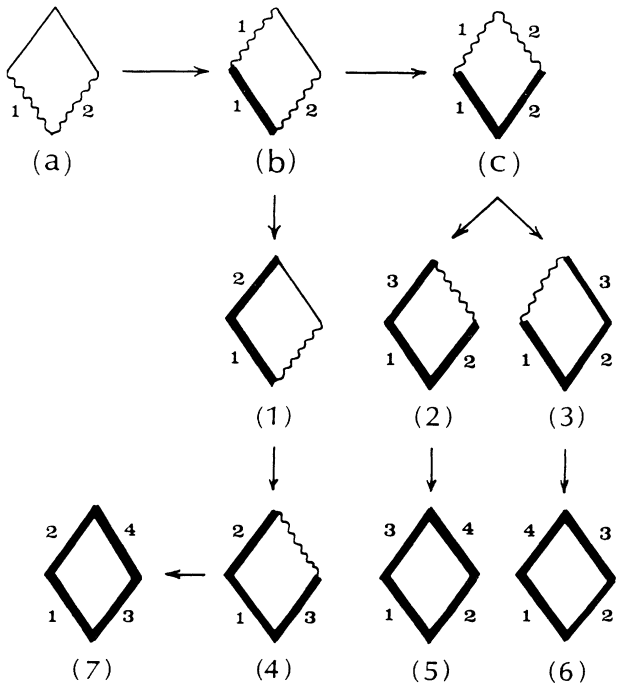

FIG. 1. All distinct configurations of the cell. The configurations (a), (b), and (c) are renormalized to growth bonds. Configurations (1)–(7) are renormalized to the injected fluid bonds. The thick, thin, and wavy lines indicate injected fluid, displaced fluid, and growth bonds, respectively.

There are three renormalization transformations. The first is for the conductance of the growth bonds,

$$\sigma_G' = \mathcal{R}_G(\sigma_G, \sigma_I, \Delta t, q_0) . \tag{4a}$$

Here the renormalization function $\mathcal{R}_G$ is the average conductance of all the nonspanning configurations that contain injected fluid bonds. The growth conductance σ_G can be interpreted as an effective conductance of a surface layer. The time increment Δt is the time period for the displacement of one injected bond.

The second renormalization transformation is for the conductance of injected fluid bonds,

$$\sigma_I' = \mathcal{R}_I(\sigma_G, \sigma_I, \Delta t, q_0) . \tag{4b}$$

Here $\mathcal{R}_I$ is the average conductance of all the spanning configurations that contain injected fluid bonds.

The third renormalization equation is for the time increment Δt. In the coarse-graining procedure, Δt (the time needed for the invading fluid to span the bond) is replaced by $\Delta t'$ (the time needed for the fluid to span the cell),

$$\Delta t' = \mathcal{R}_t(\sigma_G, \sigma_I, \Delta t, q_0) . \tag{4c}$$

Also, the renormalization equation for the total current is $q_0' = 2q_0$.

Next we discuss the renormalization functions (4a)–(4c). Figure 1 shows the breakdown process within the cell. We assume that the breakdown process occurs stepwise, with only one bond breaking at a time (no bonds break simultaneously). Configuration (a) shows a cell in which the breakdown has just reached the bottom. In configuration (b), an injected fluid bond has been added onto growth bonds 1 or 2 in configuration (a); the probability of an injected fluid bond attaching itself to these growth bonds is given by growth probabilities $p_{a,1}$ and $p_{a,2}$. The weight of configuration (b) is simply the growth probability $p_{a,1}$ multiplied by the weight of the initial configuration (a). In general, the weight of a configuration is given by the product of the growth probability.

As a first-order approximation, we assume that the currents on both sides of the diamond lattice have the same value $q_0/2$. When an injected fluid bond is added to configuration (b), configurations (c) and (1) occur. The time increases only by increment Δt. At that point, the conductance of the injected fluid bond increases,

$$\sigma_I \rightarrow \sigma_I(1 + [q\Delta t]^{\beta}) , \tag{5a}$$

where q, the current flowing on the bond, is $q_0/2$ and $\beta = \frac{3}{2}$. If we allow the breakdown to continue, the result is configuration (2) or (3). As time increases, the conductances of the injected fluid bonds increase,

$$\sigma_I \rightarrow \sigma_I(1 + [q\Delta t]^{\beta}) \rightarrow \sigma_I(1 + [2q\Delta t]^{\beta}) . \tag{5b}$$

Configurations (a)–(c) in Fig. 1 show all configurations

of the cell that can be renormalized as growth bonds.

Solving Eqs. (4a)-(4c) simultaneously, we find the three nontrivial fixed points $(1/\sigma_G^*,0,0)$, (1,1,0), and $(1/\sigma_G^*,0,1)$ in the three-parameter space $(1/\sigma_G, 1/\sigma_I, v/(1+v))$, where σ_G^* is the fixed-point value in the limiting case of an infinite viscosity ratio, and where $v \equiv q_0 \Delta t$. At fixed point (1,1,0), the growth probability becomes uniform over all the surface bonds, so the fixed point (1,1,0) corresponds to the Eden model; we call it the *Eden point.* The fixed point $(1/\sigma_G^*,0,0)$ gives a viscous finger at infinite viscosity ratio with no chemical dissolution, and is called the *first DLA point.* The fixed point $(1/\sigma_G^*,0,1)$ gives a viscous finger at infinite viscosity ratio *with chemical dissolution,* and is called the *second DLA point.*

The second DLA point can be obtained after sufficiently large time. After an infinite time, the pore size of branches in porous media becomes sufficiently large by chemical dissolution. Then the mobility of the injected fluid becomes sufficiently large. By chemical dissolution, an infinite mobility ratio can be obtained after an infinite time. Therefore the second DLA point is due to chemical dissolution, and is different from the first DLA point, which is the usual viscous fingering fixed point for a nonreactive injected fluid. The pore size of the branches in a porous medium remains at a constant value as time increases. However, at the second DLA point, the pore size of the branches is sufficiently large compared with that of the initial stages. We note that the second DLA point is distinct from the first DLA point.

We now study the stability of the fixed points in the three-parameter space. To find the global flow diagram, we choose a point in the parameter space and calculate the renormalized surface conductance, the renormalized conductance of the cluster bond, and the renormalized time increment. By using (4a)-(4c), we find a new point. We repeat this process to find the next point, and continue until we approach a stable fixed point. The renormalization flows we obtain are shown in Fig. 2. We find that the first DLA point and the Eden point are unstable fixed points, while the second DLA point is stable in all directions. All renormalization flows eventually merge into the second DLA point. From the flow diagram, we find that the double-crossover phenomena occur from the DLA fractal, through the dense pattern, and finally to the DLA fractal. The first crossover phenomena occur only when the viscosity of the reactive injection fluid is smaller than 1. In the experiment of Ref. 2, the viscosity of the reactive injection fluid is the same as that of the displaced fluid, so only the second stage of the double crossover is seen. Note that chemical dissolution inverts the direction of the crossover in the viscous fingering.

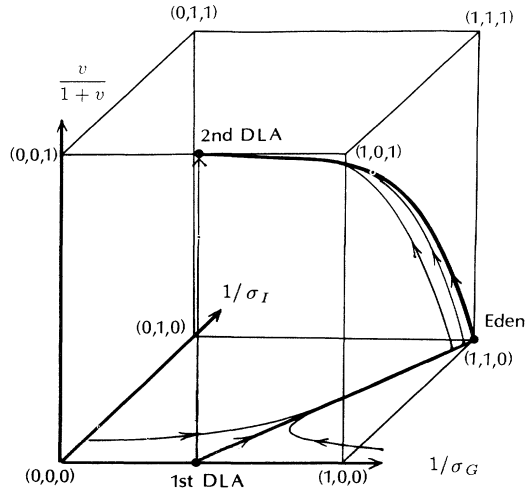

FIG. 2. Global flow diagram in three-parameter space $(1/\sigma_G, 1/\sigma_I, v/(1+v))$. There are three fixed points: the first DLA point, the Eden point, and the second DLA point. All the renormalization flows are eventually sucked into the second DLA point. In the limit $v \to 0$, viscous fingering at a finite viscosity ratio is reproduced.

For an arbitrary viscosity ratio, we propose a scaling ansatz along the crossover lines,

$$M(r,\mu,q_0,\Delta t) = r^{d_f} F_1(r^{\phi_1}/\mu) F_2(v^{1/\beta} r^{\phi_2}), \tag{6}$$

with

$$F_1(x) \sim \begin{cases} 1 & \text{if } x \ll 1, \\ x^{(d-d_f)/\phi_1} & \text{if } x \gg 1, \end{cases}$$

$$F_2(x) \sim \begin{cases} 1 & \text{if } x \ll 1, \\ x^{(d_f-d)/\phi_2} & \text{if } x \gg 1. \end{cases}$$

Here F_1 is the scaling function for the first stage of the crossover, F_2 the scaling function for the second stage of the crossover, M the mass of the cluster, r the radius of gyration, and d the embedding dimension. The scaling function for the first stage of the crossover corresponds to that of viscous fingering at a finite viscosity ratio. In an experiment with unity viscosity ratio, only the second stage of the crossover is predicted to occur.

In order to quantify this crossover behavior, we define a crossover exponent ϕ and a crossover radius r_c. We propose the following scaling ansatz along the crossover line from the Eden point to the second DLA point:

$$M(r,v) = r^d F(v^{1/\beta} r^{\phi}), \tag{7}$$

with

$$F(x) \sim \begin{cases} 1 & \text{if } x \ll 1, \\ x^{(d_f-d)/\phi} & \text{if } x \gg 1, \end{cases}$$

where the subscript 2 drops out for the scaling function and the crossover exponent. The crossover radius r_c scales as

$$r_c \sim (v^{1/\beta})^{-1/\phi}. \tag{8}$$

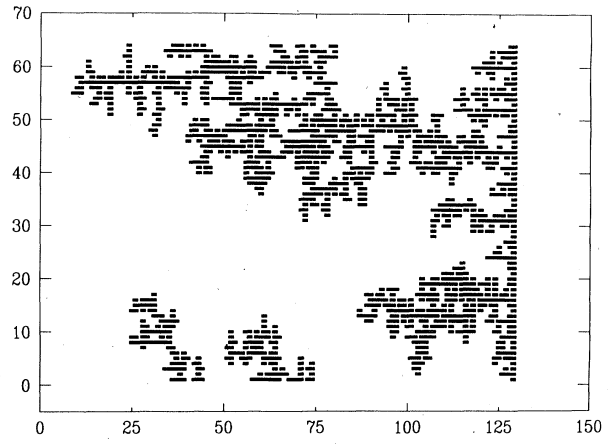

(a)

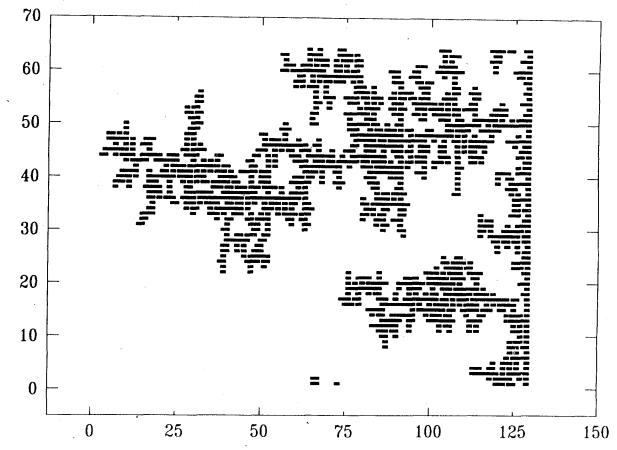

(b)

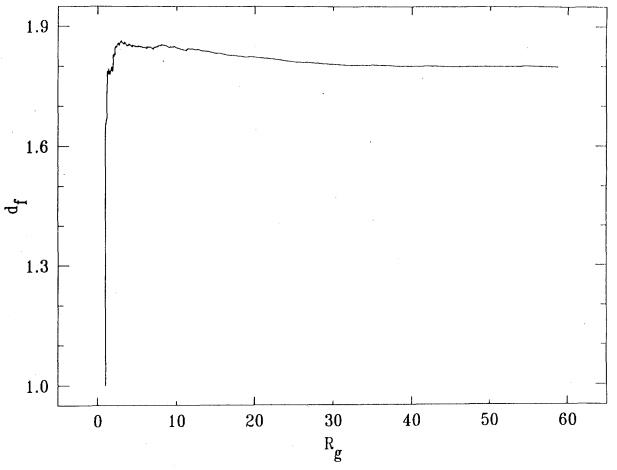

(c)

FIG. 3. Simulations for (a) $P_0=10^{-3}$ and (b) $P_0=1$ for a 128×64 square lattice, and 1000 Monte Carlo steps. (c) The dependence on cluster size of the fractal dimension d_f.

The crossover exponent ϕ is obtained by making the renormalization equations linear and calculating the eigenvalues. We obtain $\phi\simeq1.63$.

We have checked the results of the present PSRG approach for the case $\mu=1$ by direct numerical simulation. We find (1) that the asymptotic pattern is DLA, and (2) that the pattern obtained is independent of injection pressure. Our simulations were performed for a 128×64 square lattice with periodic boundary conditions in the vertical direction (Fig. 3). The pressure on the left edge is fixed at zero, and the right edge is fixed at a constant value of the applied pressure P_0. At each time step, we solve Eq. (1) by the over-relaxation method. For each interface bond i, we calculate the current q_i; we then occupy bond i with probability $q_i/\sum_j q_j$, where the index j runs over all the interface bonds. The first Monte Carlo step is completed by updating the mobility using Eq. (2).

Figures 3(a) and 3(b) show the pattern after 1000 Monte Carlo steps for the cases $P_0=10^{-3}$ and 1, respectively. We see no essential difference between these two patterns. As predicted by the PSRG, the injection pressure changes only the time scale of the pattern development. We also notice that the pattern resembles DLA. To check this possibility, we calculated the fractal dimension d_f of the pattern using the box-counting method. We find [Fig. 3(c)] that d_f approaches 1.7, consistent with known results for DLA.

This research was supported by the NSF and BP.

[1]G. Daccord, Phys. Rev. Lett. **58**, 479 (1987).

[2]G. Daccord and R. Lenormand, Nature (London) **325**, 41 (1987); see also M. L. Hoefner and H. S. Fogler, AIChE J. **34**, 45 (1988); G. Daccord, E. Touboul, and R. Lenormand, SPE Prod. Eng. **4**, 63 (1989).

[3]See, e.g., L. Paterson, Phys. Rev. Lett. **52**, 1621 (1984); M. Matsushita, M. Sano, Y. Hakayawa, H. Honjo, and Y. Sawada, Phys. Rev. Lett. **53**, 286 (1984); J. Nittmann, G. Daccord, and H. E. Stanley, Nature (London) **314**, 141 (1985); G. Daccord, J. Nittmann, and H. E. Stanley, Phys. Rev. Lett. **56**, 336 (1986); S. E. May and J. V. Maher, Phys. Rev. A **40**, 1723 (1989). See also the reviews by H. van Damme and G. Daccord in *Fractals in the Chemistry of Disordered Systems, Polymers, Colloids, and Surfaces,* edited by D. Avnir (Wiley, New York, 1989); Y. Couder, in *Random Fluctuations and Pattern Growth: Experiments and Models,* edited by H. E. Stanley and N. Ostrowsky, NATO Advanced Study Institutes Vol. 157 (Kluwer, Dordrecht, 1988); H. E. Stanely, in *Proceedings of the IUPAP International Conference on Statistical Mechanics "STATPHYS-17"* [Physica (Amsterdam) **163A**, 334 (1990)].

[4]F. Family, B. R. Masters, and D. E. Platt, Physica (Amsterdam) **38D**, 98 (1989); F. Caserta, H. E. Stanley, W. Eldred, G. Daccord, R. Hausmann, and J. Nittmann, Phys. Rev. Lett. **64**, 95 (1990).

[5]G. Daccord (to be published).

[6]See, e.g., J. Lee, A. Coniglio, and H. E. Stanley, Phys. Rev. A **41**, 4589 (1990); T. Nagatani, Phys. Rev. A **40**, 7286 (1989).